Rapid automatic multiple moving objects detection method based on feature extraction from images with non-sidereal tracking

Lei Wang,[1,2]★ Xiaoming Zhang,[1,2]★ Chunhai Bai,[3] Haiwen Xie,[2,4] Juan Li,[1,2] Jiayi Ge,[1,2] Jianfeng Wang,[1,2] Xianqun Zeng,[1] Jiantao Sun[3] and Xiaojun Jiang[1,2]★

[1] *CAS Key Laboratory of Optical Astronomy, National Astronomical Observatories, Chinese Academy of Sciences, Beijing 100101, China*
[2] *University of Chinese Academy of Sciences, Beijing 100049, China*
[3] *Xinjiang Astronomical Observatory, Chinese Academy of Sciences, Urumqi 830011, China*
[4] *Changchun Observatory, National Astronomical Observatories, Chinese Academy of Sciences, Changchun 130117, China*

Reporter: Yu Huajian

2024.12.16

Outline

1. Introduction

2. METHODS

3. RESULTS

4. CONCLUSIONS

1 Introduction

1. With the increasing emphasis on planetary defence missions and human space activities, the monitoring of natural celestial bodies (asteroids, meteors, etc.) or space objects (satellites, space debris, etc.) in near-Earth space are of great significance to the safety of human space activities (Virtanen et al. 2017).

2. Non-sidereal tracking is a common observation method, which can improve the observation accuracy and signal-to-noise ratio (SNR) of moving targets.

3. In non-sidereal tracking mode, the sensor remains pointed at the moving target. Thus, the detected moving target appears as point and stars appear as streaks. The non-sidereal tracking mode maintains the stability of a moving target within the field of view, thereby reducing image blur caused by the target's movement. Compared with the sidereal tracking mode, this improves the SNR of the target in the image (Sharma et al. 2023).

2 METHODS

$$f(x,y,k) = O(x,y,k) + S(x,y,k) + B(x,y,k) + N(x,y,k),$$

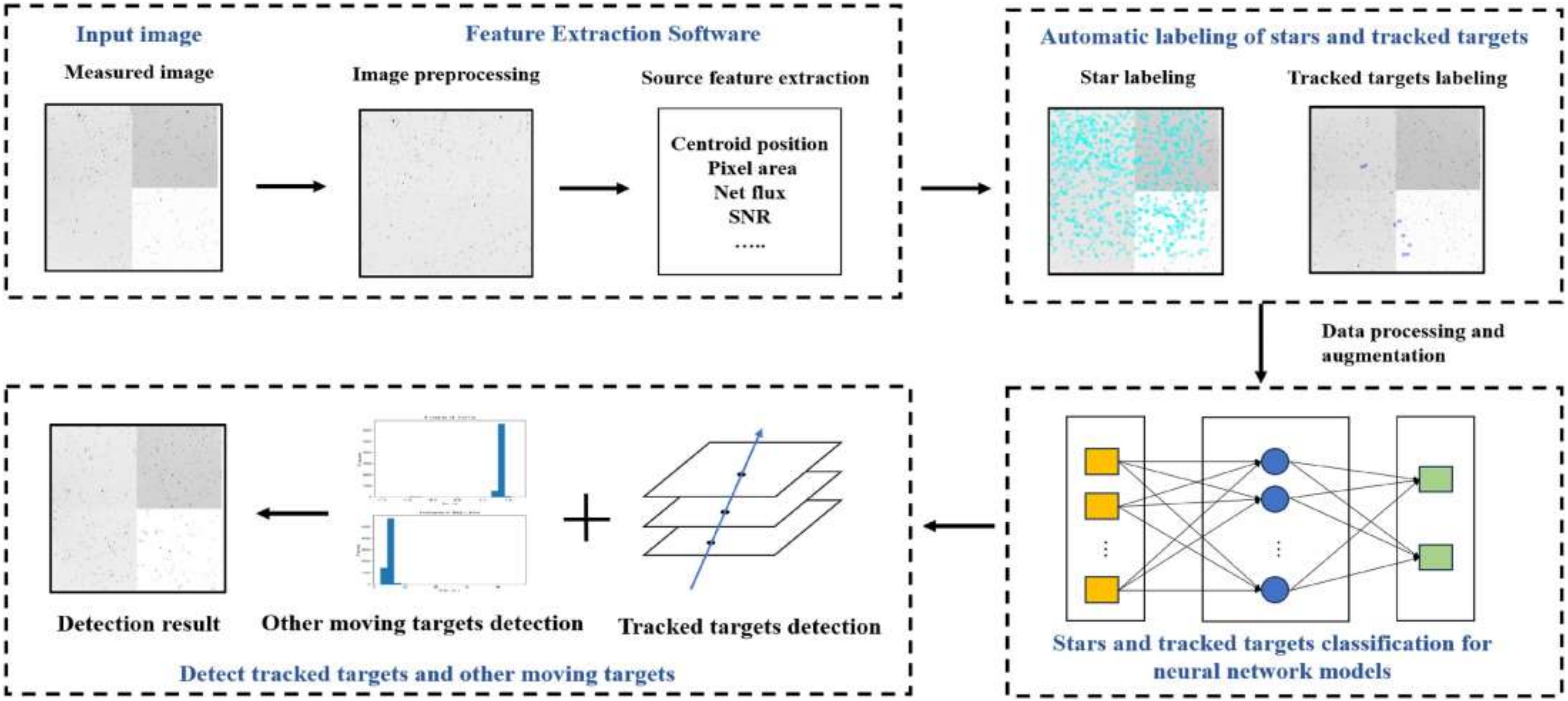

Figure 1. Algorithm flow of this article. To clearly display the sources in the image, we performed a black-and-white colour inversion on the image.

2 METHODS
Source detection and feature extraction

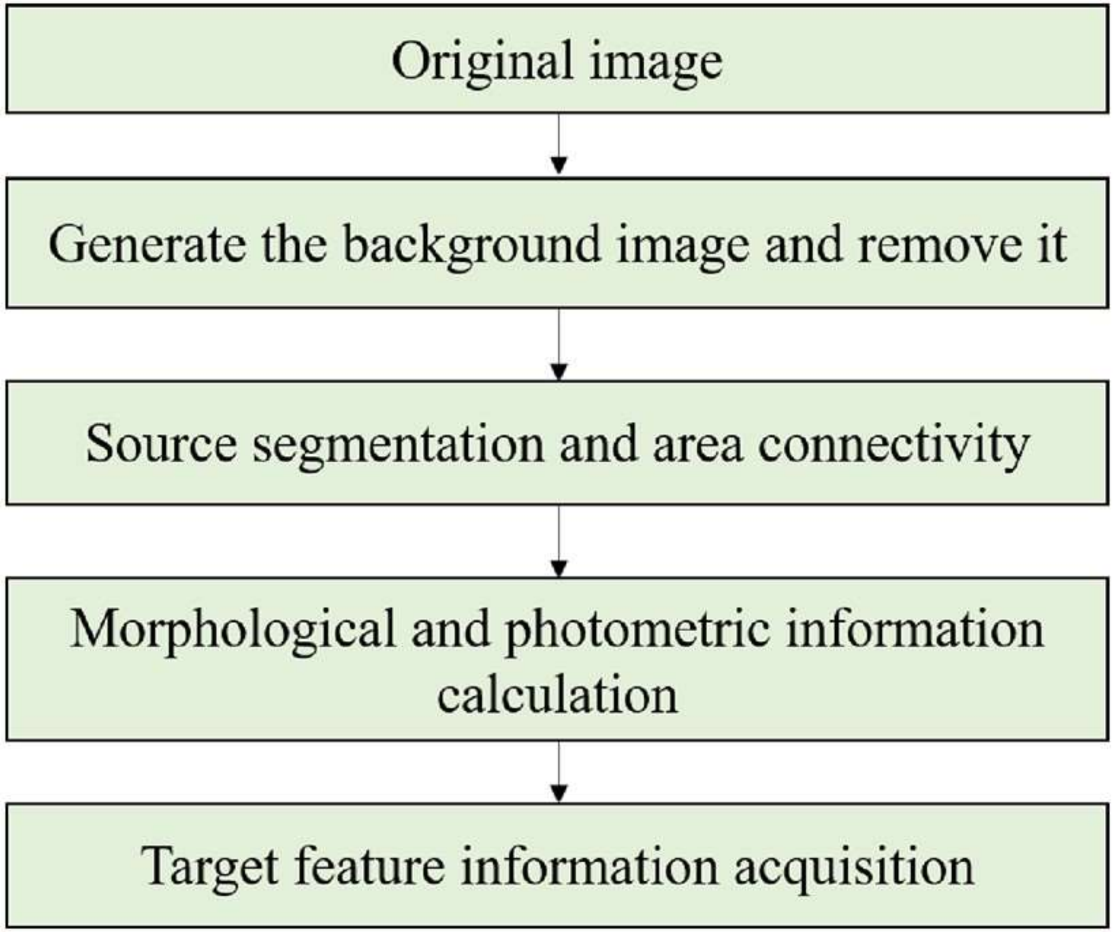

Figure 2. Feature extraction from images process in Feature Extraction Software.

2 METHODS

Source segmentation and extraction

The formula for calculating the circularity *C* of the contour of the connected region is as equation:

$$C = \frac{b}{a},$$

where *a* is the major axis length, and *b* is the minor axis length. When the target area is circular, the circularity value is maximum, i.e. 1.

The inclination angle θ of the connected domain is calculated as equation :

$$\theta = \pm \arctan\left(\frac{y_2 - y_1}{x_2 - x_1}\right),$$

where (x1, y1) and (x2, y2) are the coordinates of the two endpoints of the connected domain in the direction parallel to the major axis.

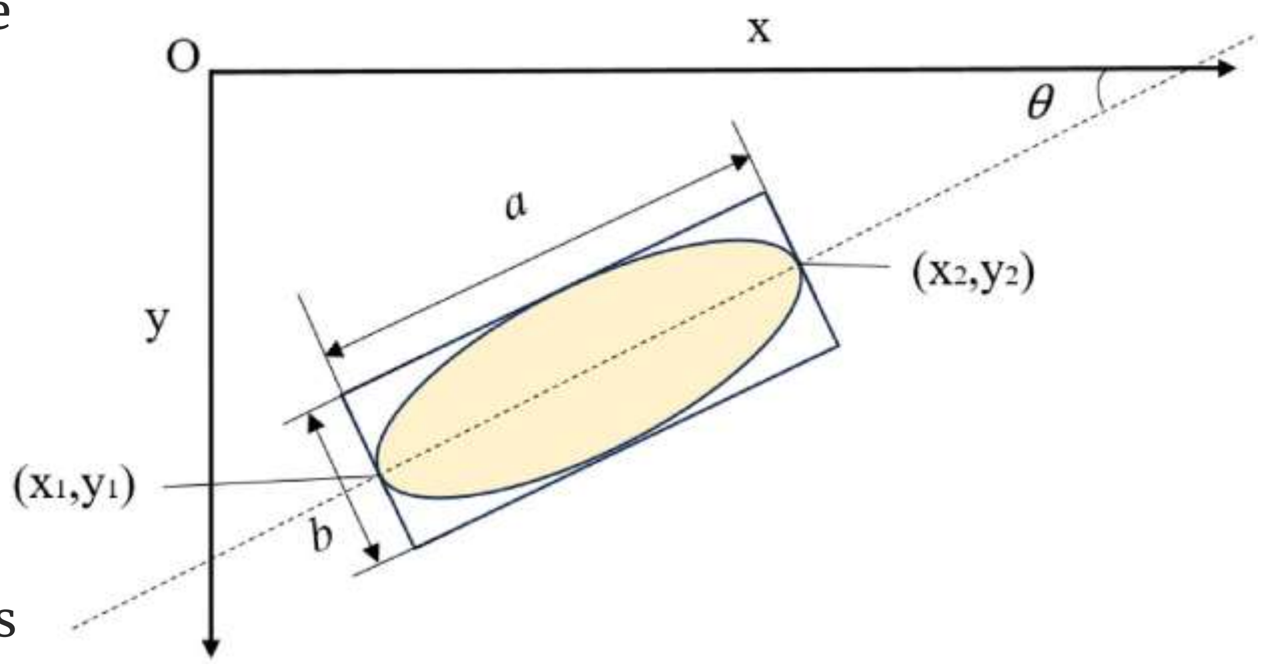

Figure 3. Morphological information of the connected regions. Here, O is the origin of the pixel coordinate system, a is the major axis length, b is the minor axis length, and θ is the inclination angle. The sign is positive clockwise along the x-axis, negative otherwise. (x1, y1) and (x2, y2) are the coordinates of the two endpoints.

2 METHODOLOGY

Source centroid position calculation and flux measurement

The centroid method (Horn 1986; see equation 5) is used to calculate the centre of the source and the aperture photometry method (Laher et al. 2012) to obtain the flux information of the source in this paper. At the same time, luminance information such as instrument magnitude and background luminance is calculated. We calculate the SNR according to equation :

$$(x_0, y_0) = \frac{\left(\sum_{(x,y)\in S}(x,y)I(x,y)\right)}{\left(\sum_{(x,y)\in S} I(x,y)\right)}.$$

$$SNR = \frac{F \times \sqrt{S}}{\sigma_{\mathrm{b}}},$$

where (x0,y0) is the centroid of source, *S* is source area after segmentation, I(x,y) is the brightness of the original image at (x,y), *F* is the flux of the source, and σb is the standard deviation of the background.

2 METHODS

Feature Extraction Software

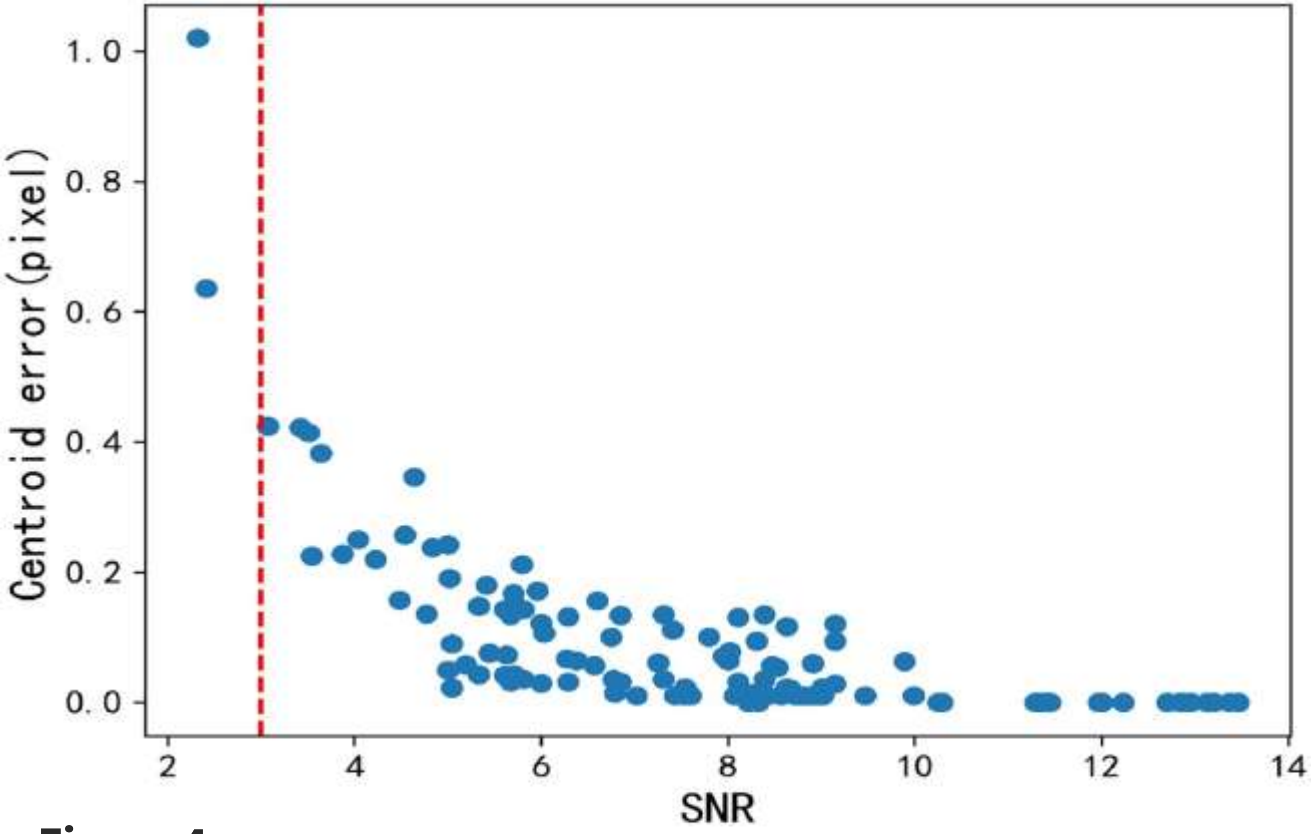

Figure 4.
Centroid detection accuracy distribution of simulated targets (FWHM = 5 pixels) with different SNR in Feature Extraction Software. The horizontal axis represents the SNR of the source, the vertical axis represents the centroid error extracted by the Feature Extraction Software from the source. The dash vertical line represents an SNR of 3.

Table 1.
Features extracted by Feature Extraction Software and their definitions.

Feature	Definition
Frame	The number of frames of the image
Img-*x*	Centre point *x* coordinates of the source
Img-*y*	Centre point *y* coordinates of the source
Pixels-*N*	Pixel area of the source
Flux	Flux of the source
INST-mag	Instrument magnitude of the source
SNR	SNR of the source
Pix-flux-peak	Single pixel peak flux within the region of the source
Pix-flux-bk	Source area background single pixel flux
Major	The major axis length of the source
Minor	The minor axis length of the source
Circularity	The circularity of the source
Incline	The inclination angle of the source

2 METHODS
Feature Extraction Software

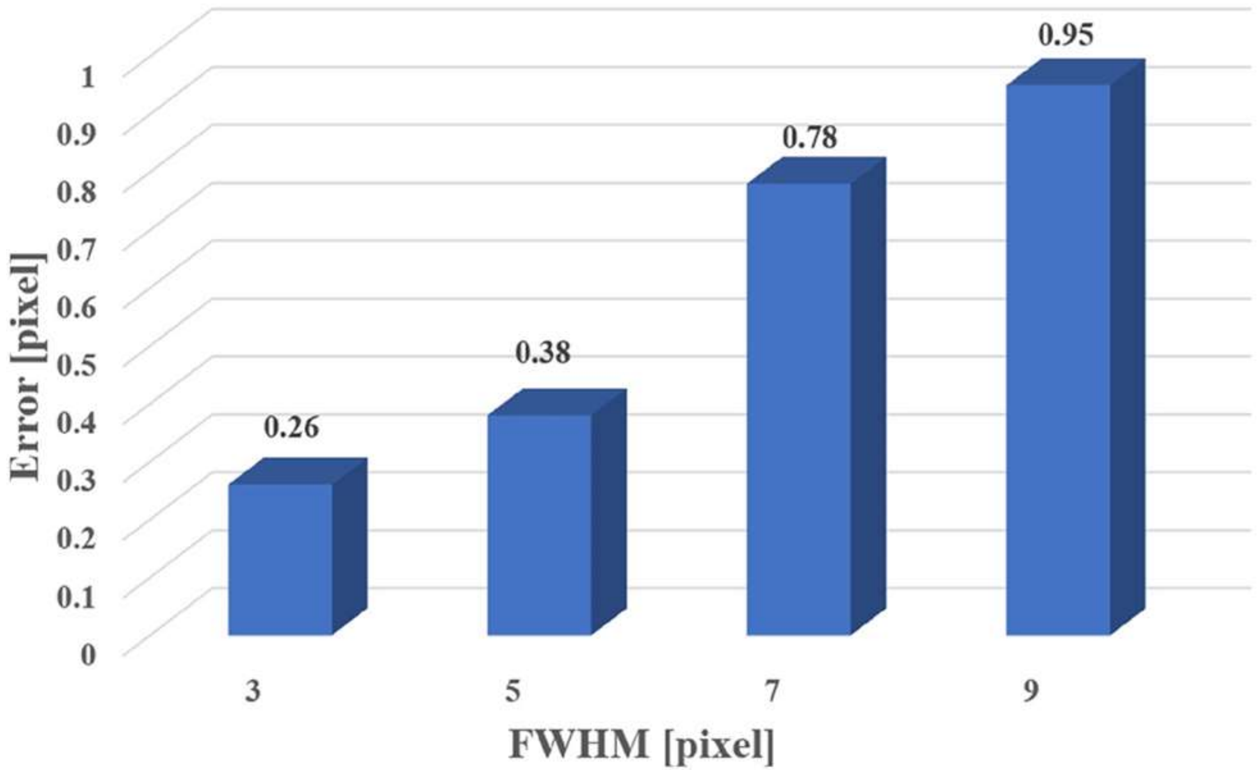

Figure 5.
The variation of average centroid error for simulated point targets with different FWHM values, where the SNR of the targets ranges from 3 to 6.

Table 1.
Features extracted by Feature Extraction Software and their definitions.

Feature	Definition
Frame	The number of frames of the image
Img-*x*	Centre point *x* coordinates of the source
Img-*y*	Centre point *y* coordinates of the source
Pixels-*N*	Pixel area of the source
Flux	Flux of the source
INST-mag	Instrument magnitude of the source
SNR	SNR of the source
Pix-flux-peak	Single pixel peak flux within the region of the source
Pix-flux-bk	Source area background single pixel flux
Major	The major axis length of the source
Minor	The minor axis length of the source
Circularity	The circularity of the source
Incline	The inclination angle of the source

2 METHODS

Moving object detection

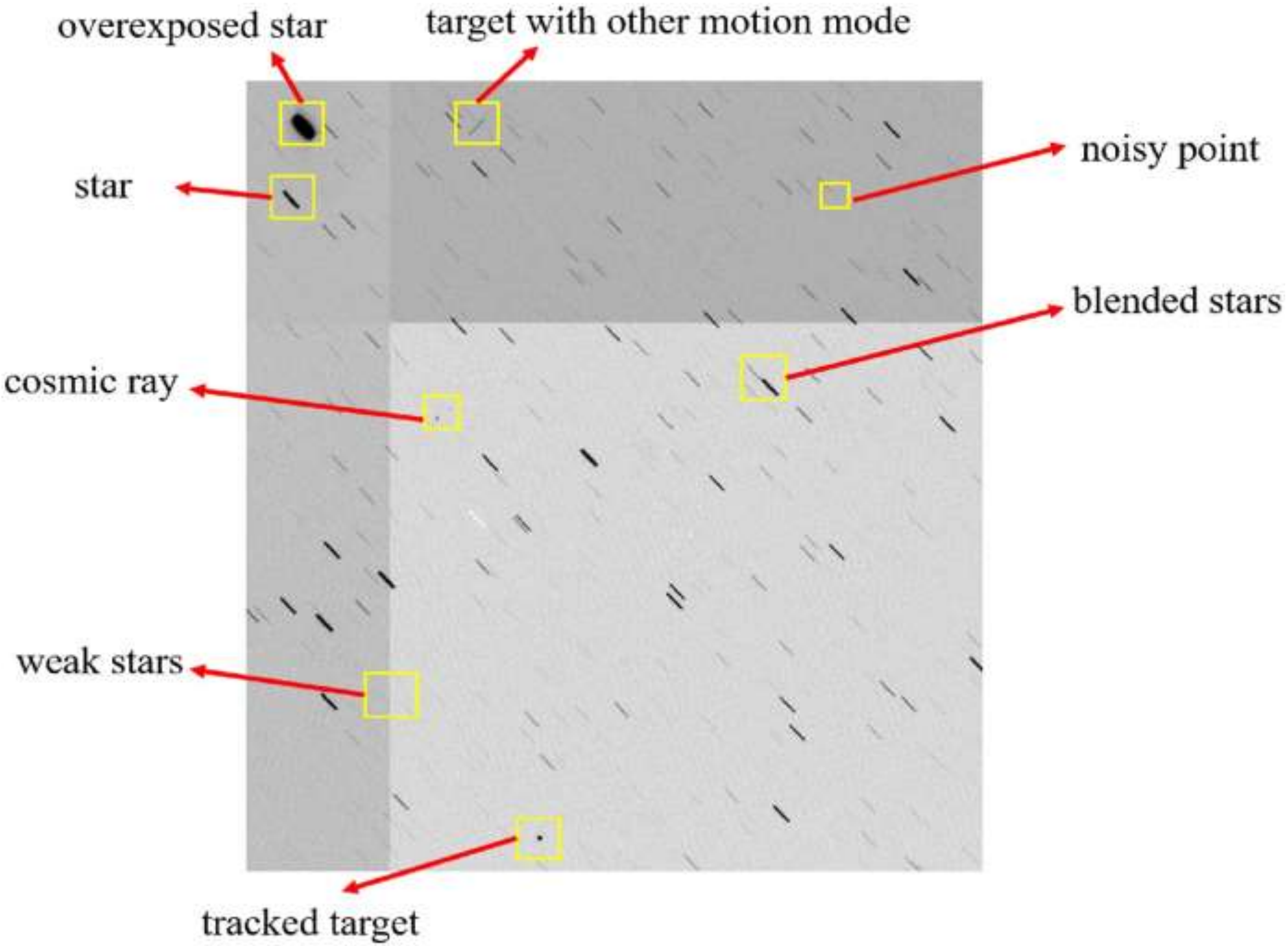

Figure 6.

The types of source extracted from the image include stars (weak stars, blended stars, and overexposed stars), moving objects (TTs and TOMs), noisy points, cosmic rays, etc. The image is sourced from *Nanshan One-meter Wide-field Telescope* and has been cropped. We performed a black-and-white colour inversion on the image.

2 METHODS

A naive method for classifying stars and TTs

Figure 7.
Moving object matching diagram. *O*1, *O*2, and *O*3 are the centre positions of the matched target sources. The neighbourhood *R* serves as the search range for target matching. When points in the next frame of the image fall within the *R* region, they are considered as potential candidate targets. Only when a target is successfully matched in three consecutive frames of images, it is deemed to be the same target across different frames of the image. In target tracking mode, the distance between *O*1, *O*2, and *O*3 is very close.

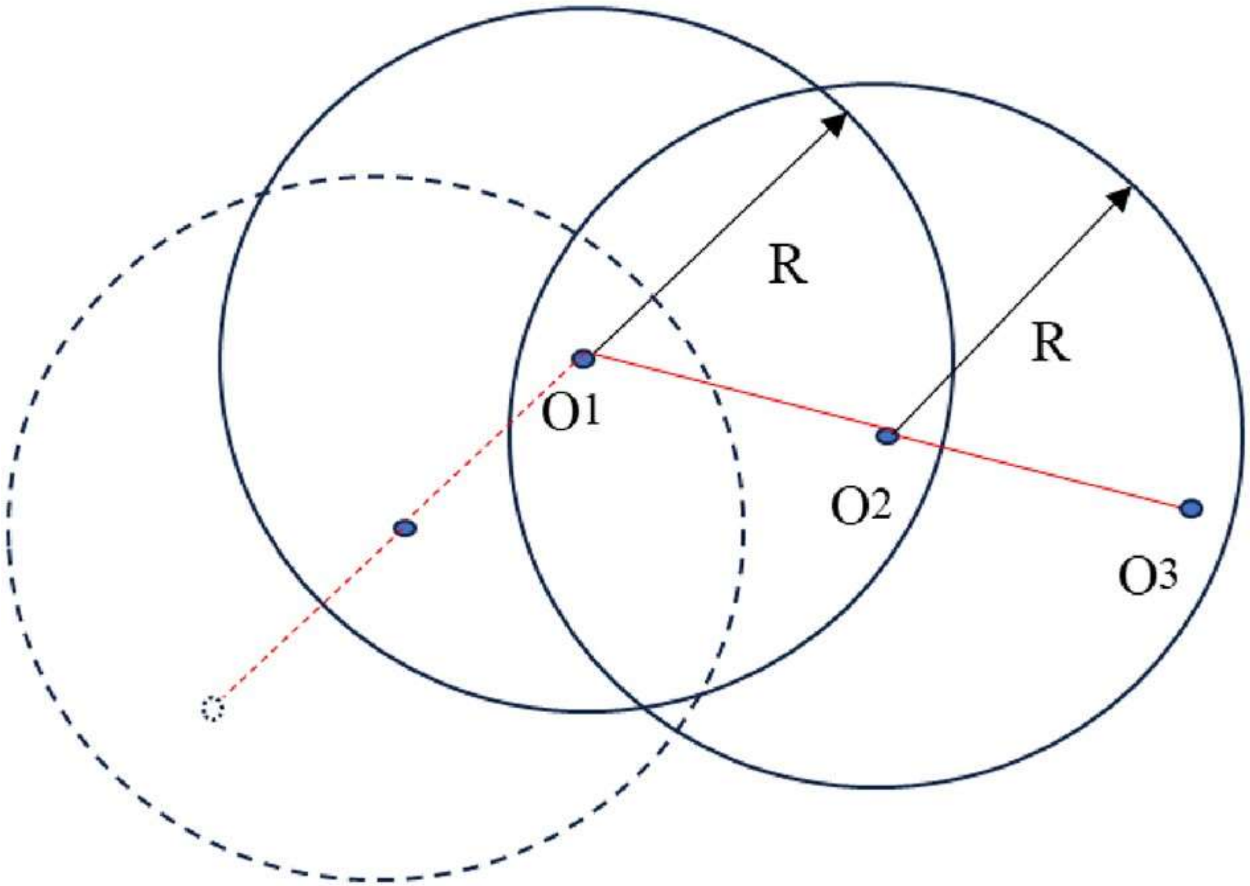

2 METHODS

Neural network classifies stars and TTs

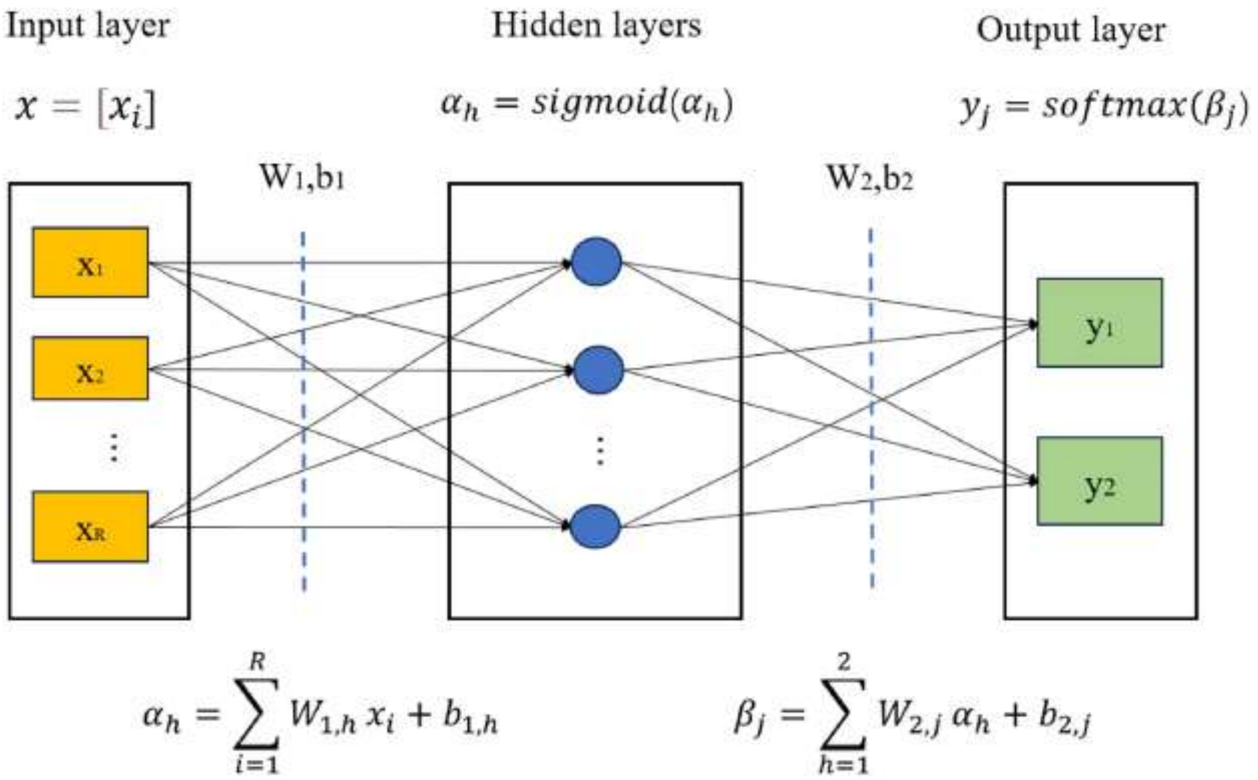

The structure of the neural network in this paper. The neural network is used to classify object by their extracted features.

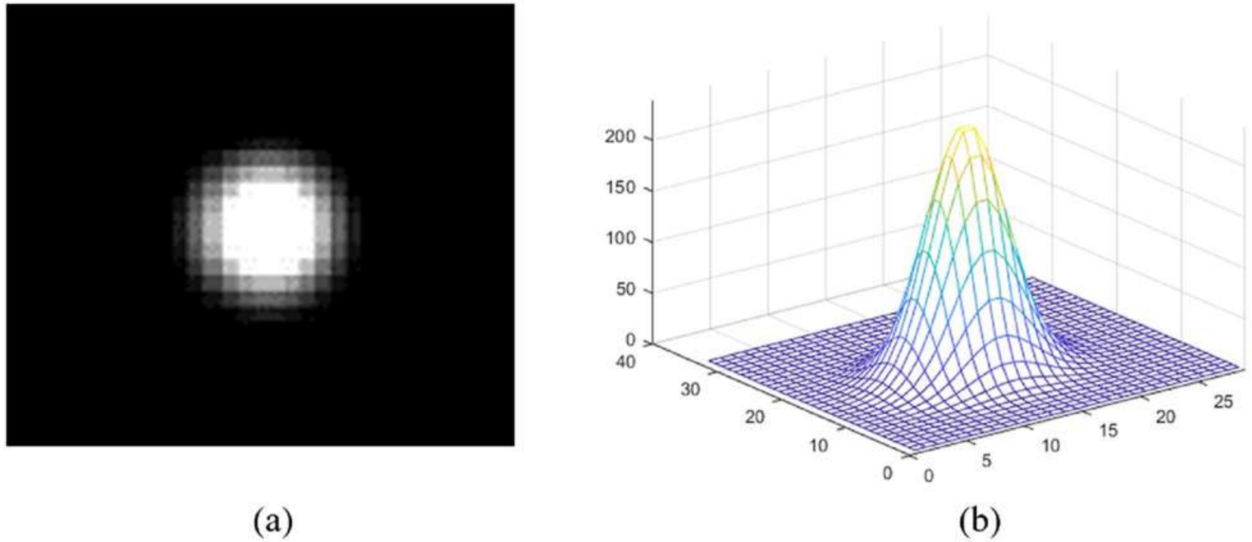

Simulation of TT image by 2D Gaussian function. (a) 2D diagram of simulated target. (b) 3D brightness distribution diagram of simulated target.

2 METHODS
Further detection of moving targets

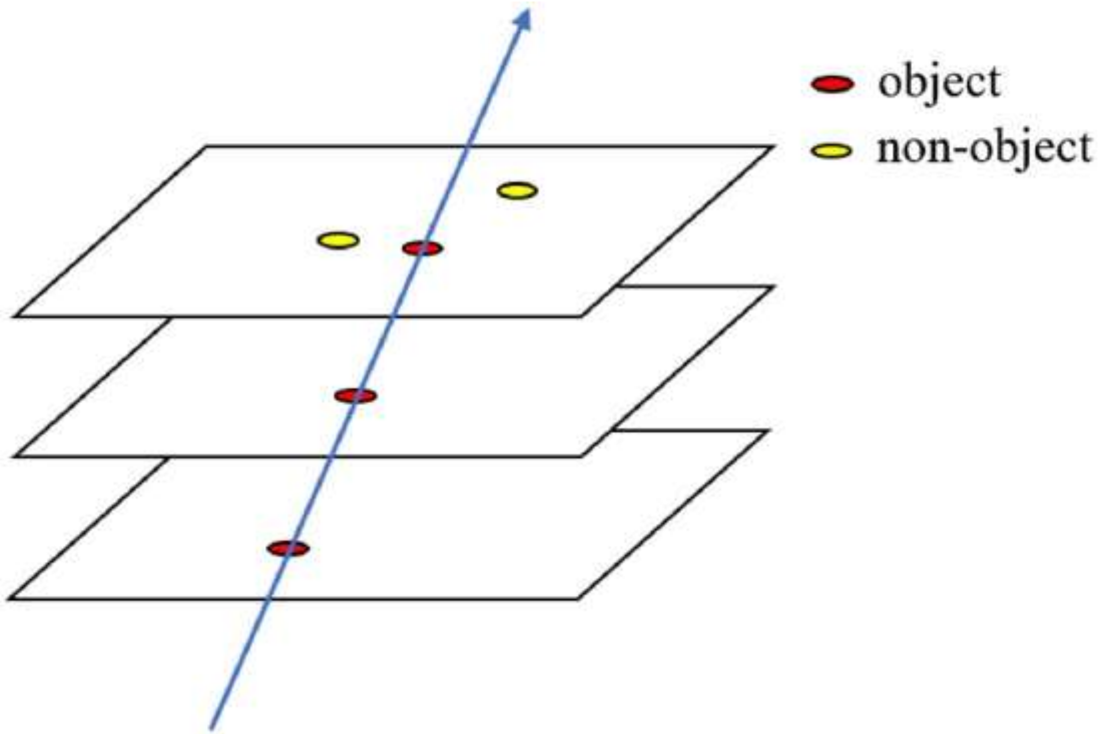

Figure 10.The method of continuous multiframe track association is used to judge the moving object. For the image of target tracking mode, the target motion track is almost a vertical line.

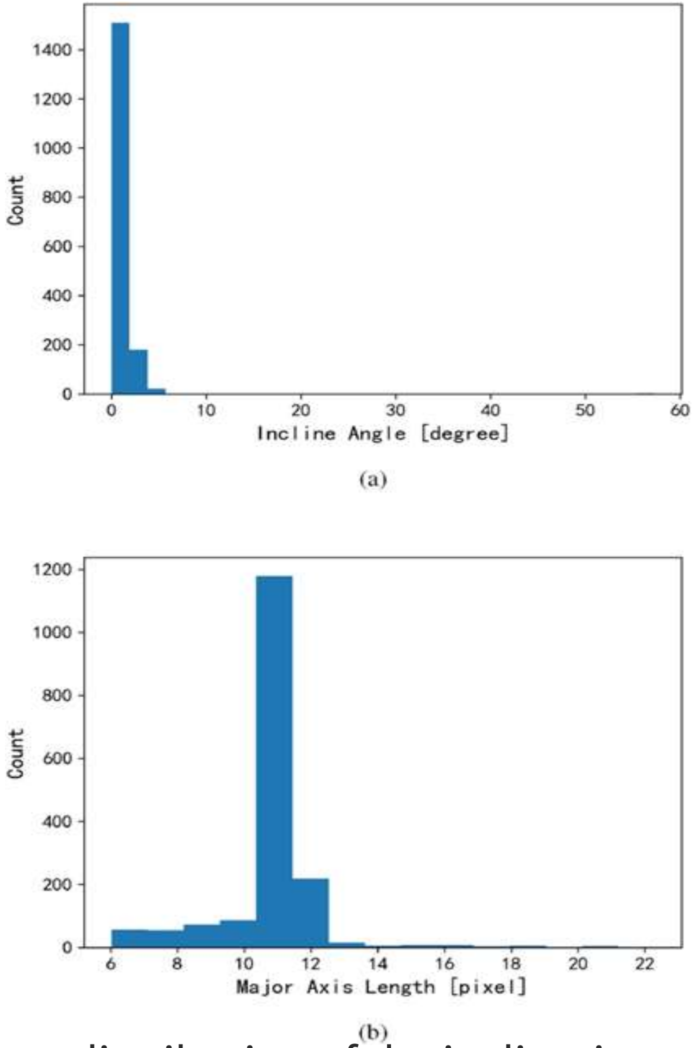

Figure 11.Histogram distribution of the inclination angle (a) and major axis length (b) of the striped target detected using the neural network model in a single frame image from *Nanshan One-meter Wide-field Telescope*, with a bin = 30 for inclination angle and bin = 15 for major axis length.

3 RESULTS
Experimental setting

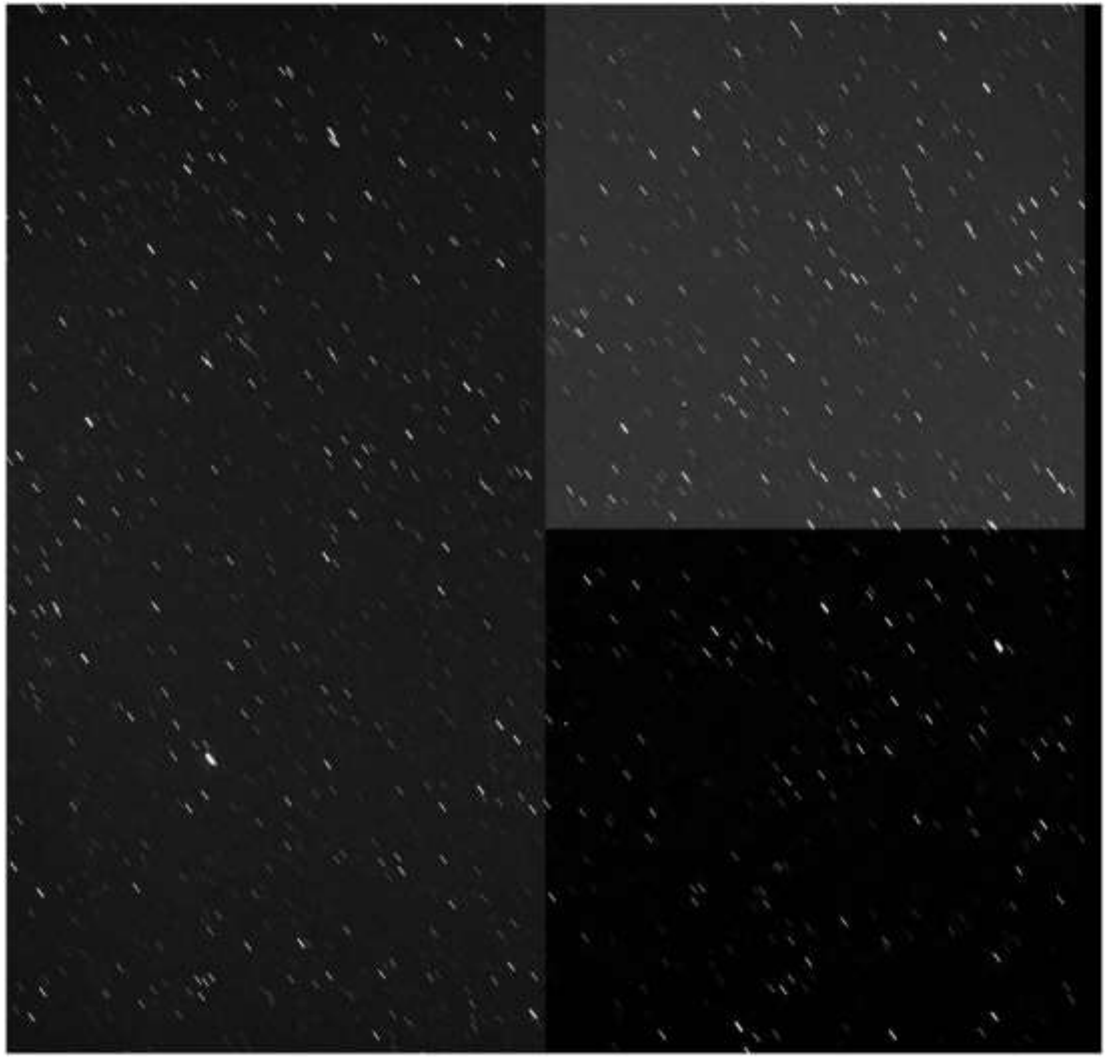

Table 3.
The relevant parameters of *Nanshan One-meter Wide-field Telescope* and its detectors.

Features	Characteristics
Effective diameter	1000 mm
Prime focal length	2200 mm
FOV at prime focus	$1.5^\circ \times 1.5^\circ$
Primary mirror reflectance	87 per cent
Primary mirror material	Schott Zerodur
CCD pixel number	4096×4136
CCD pixel size	$12\,\mu m \times 12\,\mu m$
CCD pixel scale	1.125 arcsec
Dark current $(e^{-}\mathrm{pixel}^{-1}\,\mathrm{h}^{-1})$	3 @ − 100°C, 0.01 @ −120°C
Readout noise	$3 \sim 4.5\,e^{-}$
Full frame readout time	27s@146 kHz, 44s@91 kHz, 78s@51 kHz
Linearity	>99.9995 per cent

Figure 12. An image of space objects captured by *Nanshan One-meter Wide-field Telescope* at the Nanshan Observatory of the Xinjiang Astronomical Observatory in 2018 June. The image has not undergone bias and flat-field correction.

3 RESULTS

Experimental setting

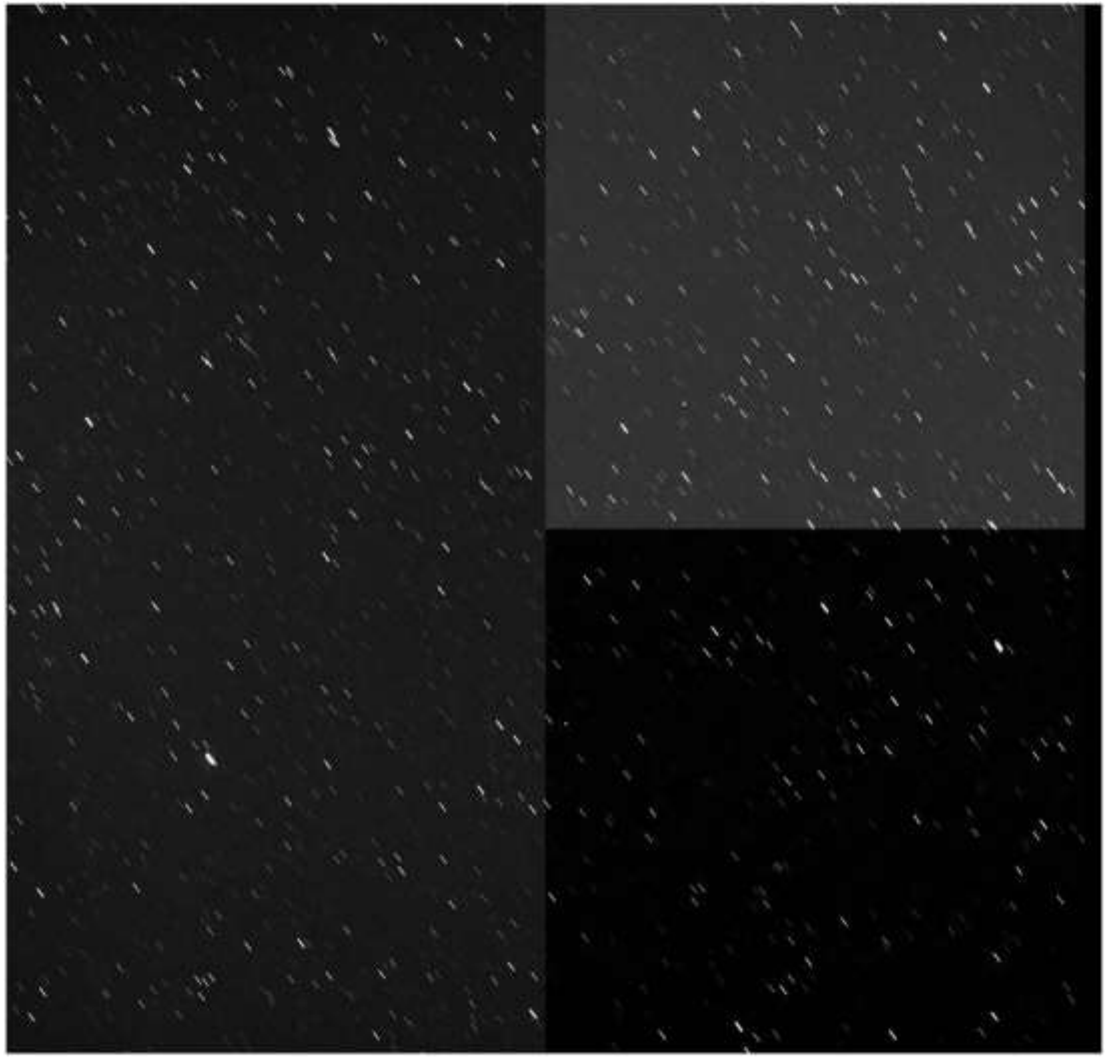

Image source	Number of real TTs
The first 99 frames of 129 images	360
The last 30 frames of 129 images	141
62 frames of continuous observation	62
21 frames of continuous observation	42

Table 4. The number of real TTs in experimental images, where the count is determined manually. The 129 images in the table refer to 129 frames from 43 different sky regions for observation.

3 RESULTS

Feature extraction based on the Feature Extraction Software

Table 5.

Partial feature data extracted from the Feature Extraction Software.

Frame	Img-*x*	Img-*y*	Pixels-*N*	Flux	INST-mag	SNR	Pix-flux-peak	Pix-flux-bk	Major	Minor	Circularity	Incline
1	2092.4	2781.6	128	170 067.0	13.1	403.7	16 304.0	57.8	1.6	1.5	0.96	0.75
55	2570.0	3361.0	89	62 475.9	14.2	239.1	4864.6	65.0	1.6	1.6	0.99	0.88
16	823.8	602.3	322	571 501.3	11.8	741.6	43 405.3	69.5	1.9	1.7	0.89	0.87
13	2864.5	1423.3	6546	23 641 728	7.8	4784.2	54 988.1	118.8	20.1	5.7	0.28	1.40
17	1146.0	4129.4	2369	138 600.8	13.3	302.3	510.5	30.2	96.0	4.2	0.04	0.09
58	4091.3	3023.1	13	617.8	19.2	18.0	84.4	43.2	1.3	1.3	0.25	0.79
9	2366.5	242.5	1583	9797 929	8.7	3111.7	55 034.2	73.9	11.6	2.0	0.17	1.11
1	2502.8	3281.5	91	63 821.1	14.2	240.3	5281.9	73.9	1.6	1.6	0.40	0.88
2	2128.3	2867.6	971	2681 195.8	10.1	1619.7	21 457.9	60.9	12.0	2.0	0.17	1.12
81	1555.4	3503.9	281	855 806.3	11.4	908.3	55 004.8	113.6	1.8	1.8	0.98	0.76
…	…	…	…	…	…	…	…	…	…	…	…	…

3 RESULTS
Automatic labelling of stars and TTs

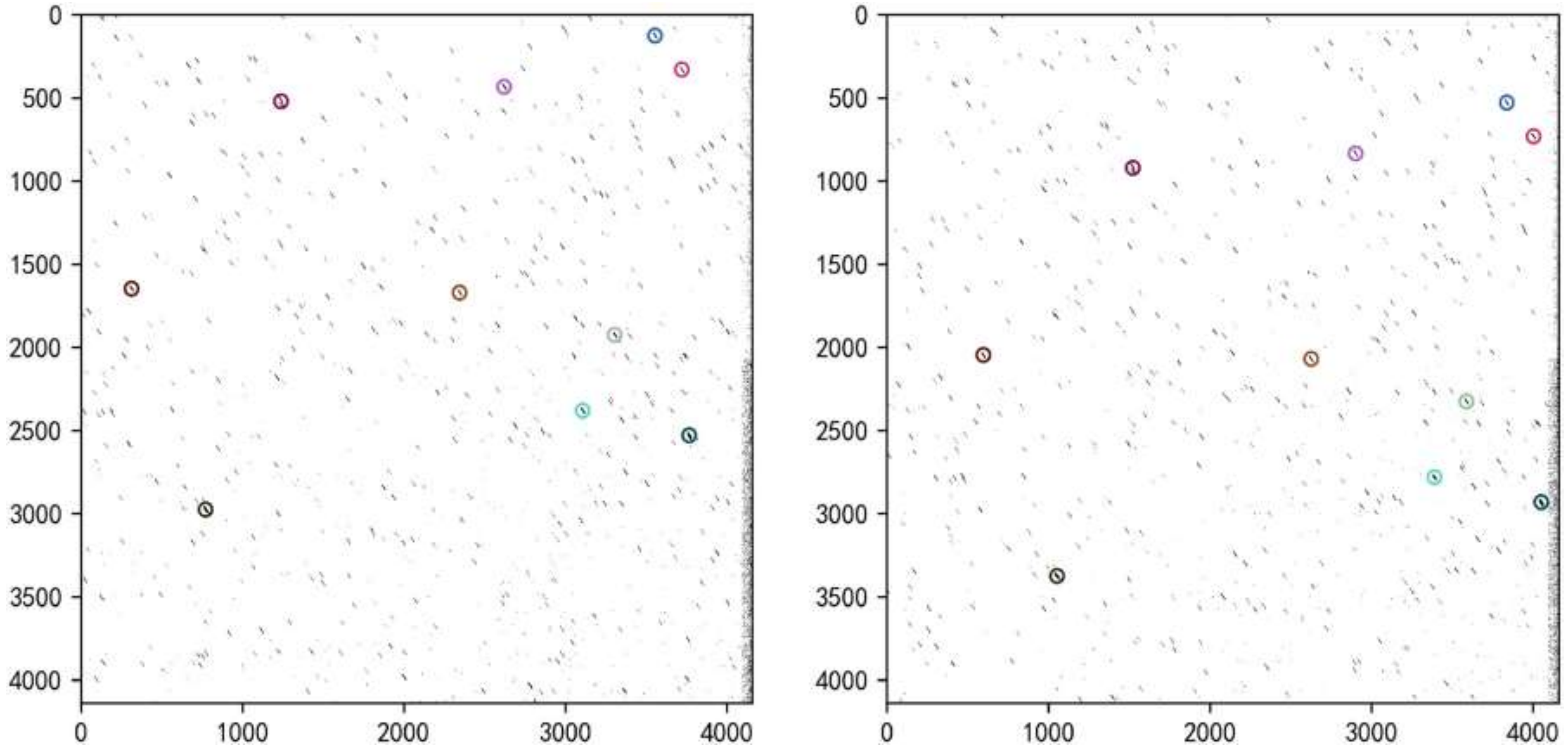

Figure 13. Star align based on image registration. Left and right are two consecutive frames of observation images, and the circles in the image mark the 10 brightest stars in terms of flux. The circle of the same colour in the left and right images represents the same star matched. We performed a black-and-white colour display and inversion on the image.

3 RESULTS

Classification of stars and TTs based on neural network method

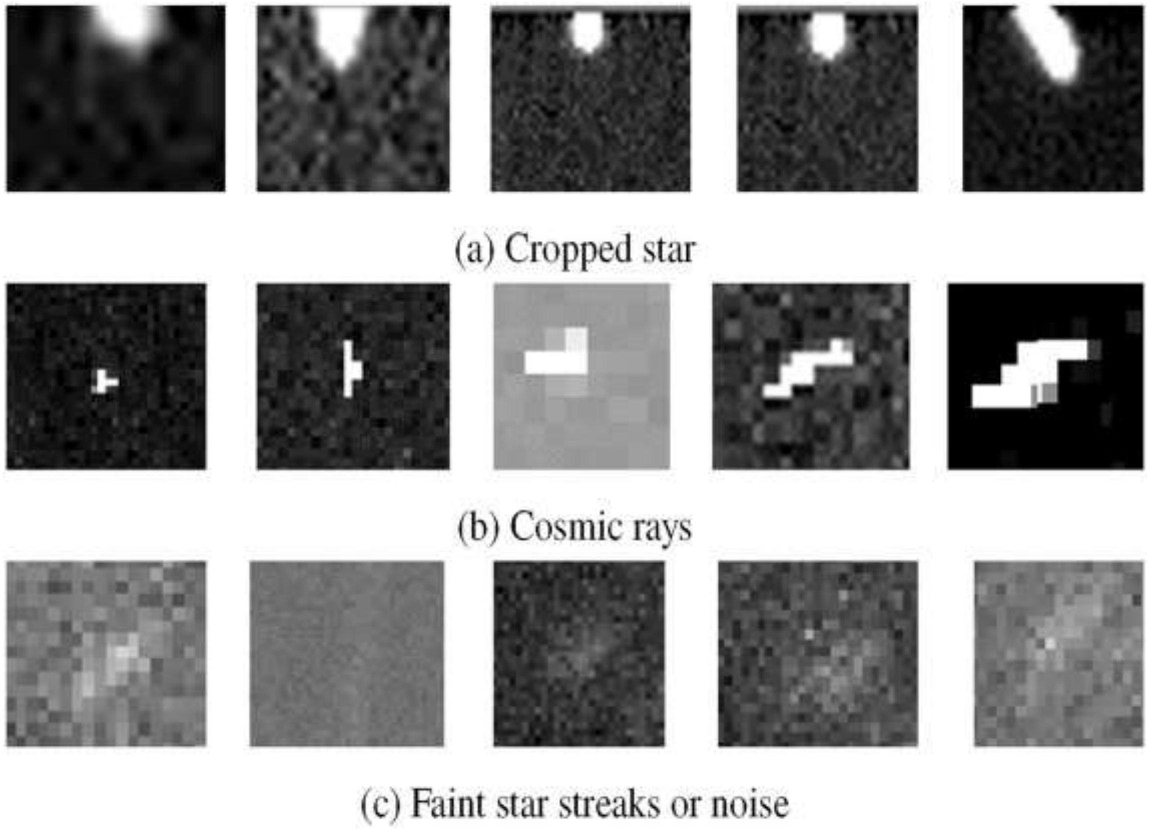

Figure 16. The image shows the types of point-like targets detected by the neural network model in the validation data set, excluding the TT.

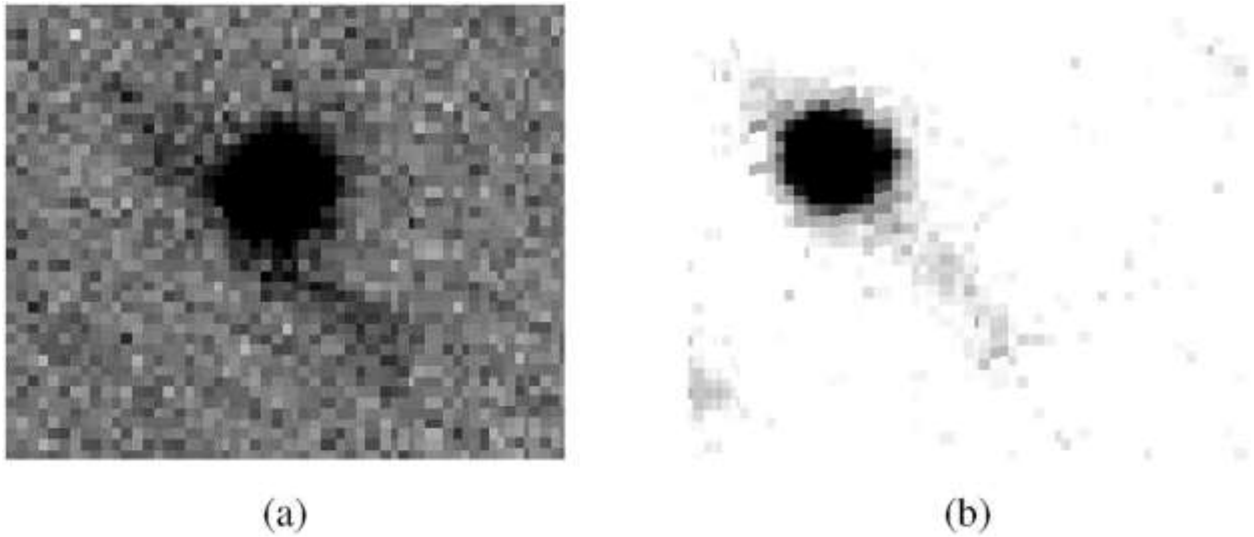

Figure 18. Images of star overlapping with object. In this case, it is difficult for the neural network model to detect the targets.

3 RESULTS

Classification of stars and TTs based on neural network method

Method	P_d	FAR	Time
This paper	97.55 percent	0	0.33 s
A naive method	73.47 percent	23.67 percent	7.01 s

Table 8.

		Detection	
	Class	TOM	Other
Ground truth	TOM	30	9
	Other	15	–
P_d		76.92 percent	
FAR		27.78 percent	

Table 9. Detection results of TOMs in validation data set

3 RESULTS

Results and analysis

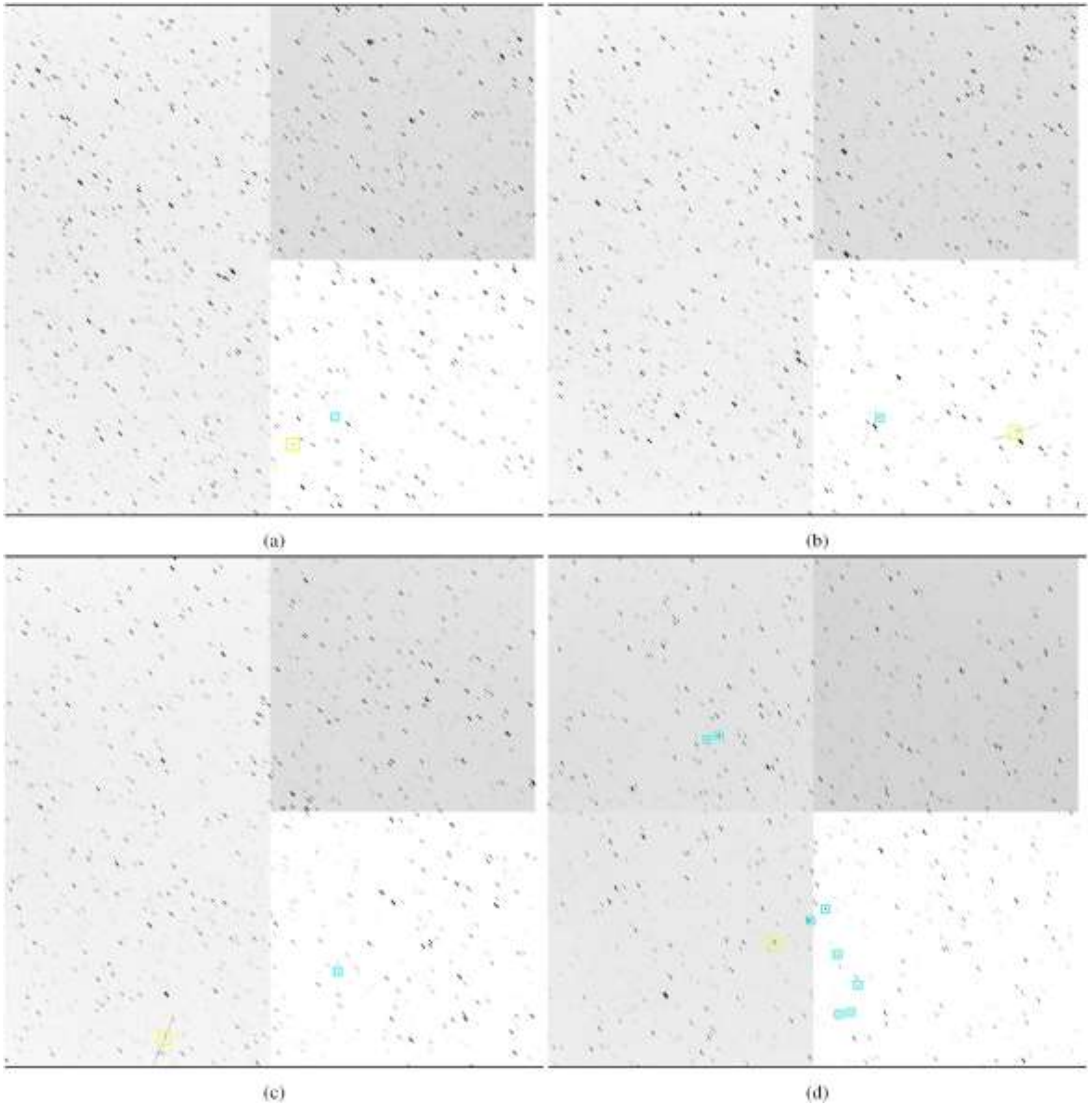

	Detection			
	Class	TT	TOM	Other
Ground truth	TT	239	0	6
	TOM	0	30	9
	Other	0	15	–
P_d		94.72 per cent		
FAR		5.02 per cent		

Table 10. Detection results of all types of moving objects, TTs, TOMs, and others in validation data set.

Figure 19. The display of the detection result in the original image, where the target in the smaller box represents the TT, and the target in bigger is the TOM. We performed a black-and-white colour inversion on the image.

4 CONCLUSIONS

Our main results are summarized below:

Feature information is extracted from optical images, and the stars and TTs are automatically labelled. Then, the data are trained by the fully connected neural network model, and the classification results are obtained according to the model, and the TTs are detected by KD-Tree track association, and TOMs are detected by statistics of inclination angle and major axis length data.

1.The method can, not only accurately detect the TT in the image and the target with the same speed as the TT, but also realizes the detection of other targets with moving modes in the image.

2.The neural network model in this method uses the data extracted from images for training and can obtain good training effects. This demonstrates that the model can be effectively trained without the accumulation of excessive data in the image samples, enabling the algorithm to achieve satisfactory training outcomes even with a limited number of observational images. This method has a small amount of computation, not only can enhance the adaptability of the system, but also can apply the network to real-time data processing.

3.Looking ahead, we will continue to deepen our research and apply more experimental data to various practical scenarios to validate and optimize our algorithm. At the same time, we will also focus on the impact of overexposed stars in images and the detection of fast-moving objects, and consider using more accurate feature information such as FWHM and more accurate SNR formulas to improve the accuracy and adaptability of the moving objects detection algorithm.

Thanks